

Tracking fin whales in the northeast Pacific Ocean with a seafloor seismic network

William S. D. Wilcock^{a)}

School of Oceanography, University of Washington, Seattle, Washington 98195-7940

(Received 27 September 2011; revised 27 July 2012; accepted 2 August 2012)

Ocean bottom seismometer (OBS) networks represent a tool of opportunity to study fin and blue whales. A small OBS network on the Juan de Fuca Ridge in the northeast Pacific Ocean in ~ 2.3 km of water recorded an extensive data set of 20-Hz fin whale calls. An automated method has been developed to identify arrival times based on instantaneous frequency and amplitude and to locate calls using a grid search even in the presence of a few bad arrival times. When only one whale is calling near the network, tracks can generally be obtained up to distances of ~ 15 km from the network. When the calls from multiple whales overlap, user supervision is required to identify tracks. The absolute and relative amplitudes of arrivals and their three-component particle motions provide additional constraints on call location but are not useful for extending the distance to which calls can be located. The double-difference method inverts for changes in relative call locations using differences in residuals for pairs of nearby calls recorded on a common station. The method significantly reduces the unsystematic component of the location error, especially when inconsistencies in arrival time observations are minimized by cross-correlation.

© 2012 Acoustical Society of America. [<http://dx.doi.org/10.1121/1.4747017>]

PACS number(s): 43.60.Jn, 43.30.Sf, 43.80.Ka [AMT]

Pages: 2408–2419

I. INTRODUCTION

Passive acoustic monitoring is an important tool for studying the distribution and abundance of large whales in the oceans, characterizing their behavior and habitat usage, and assessing how they are impacted by anthropogenic sounds (Zimmer, 2011). Long term studies lasting a year or more can be used to assess seasonal variations in whale distribution and behavior. In some locations, permanent networks of sensors are available for such studies but in most places autonomous instruments are required. A number of instruments have been developed or adapted for monitoring whales with hydrophones either deployed near the seafloor (Clark *et al.*, 2002; Wiggins, 2003; Greene *et al.*, 2004; Lammers *et al.*, 2008) or on moorings (Fox *et al.*, 2001; Moore *et al.*, 2006; Ioup *et al.*, 2009). Such specialized recording packages can be costly to deploy and recover, particularly in locations that require the use of a dedicated research vessel. It is thus advantageous to find experiments of opportunity to monitor whales.

Ocean bottom seismometers are designed to record earthquakes and anthropogenic sounds with a sensor package that comprises three orthogonal seismometers that measure ground velocity and may also include a hydrophone or long-period pressure sensor. Networks of OBSs are increasingly being deployed for a year or more to monitor seismicity in tectonically active regions. The bandwidths of OBSs typically extend up to ~ 50 Hz and are thus sufficient to record the low-frequency calls of the two largest baleen whale species, blue and fin whales. Several studies have demonstrated the potential of OBS networks to determine the tracks and calling patterns of blue and fin whales (McDonald *et al.*,

1995; Rebull *et al.*, 2006; Dunn and Hernandez, 2009; Frank and Ferris, 2011). However, the OBS studies of fin and blue whales to date have been limited to a few sequences and the onset times required for tracking have been identified and analyzed manually. This paper describes and shows examples of techniques to track fin whales that have been developed to facilitate the analysis of an extensive data set of fin whale calls recorded by a seafloor seismic network in the NE Pacific Ocean.

II. SEISMIC NETWORK AND DATA

The seismic network used for this study was deployed from 2003–2006 on the central part of the Endeavour segment of the Juan de Fuca ocean-spreading ridge (Fig. 1). Seafloor depths in the area range between 2000 and 2800 m and the bathymetry near the network is characterized by ridge parallel hills with a dominant wavelength of ~ 7 km and an amplitude of ~ 300 m. The seafloor is composed of rough basaltic flows along the spreading center and topographic highs with a thin sediment cover in topographic lows and a more extensive sediment cover by Pleistocene turbidities to the east of the ridge axis (e.g., McManus *et al.*, 1972; Karsten *et al.*, 1986).

The network (Fig. 1) comprised eight OBSs and extended about 10 km along the ridge axis and 6 km across. The objective of the experiment was to monitor microearthquakes associated with hydrothermal heat extraction from a crustal magma chamber at 2–3 km depth (Wilcock *et al.*, 2009). The instrument spacing of ~ 3 km reflects the desire to have the nearest instrument no further away from the epicenter than the focal depth beneath the seafloor in order to resolve the earthquake location well (Lee and Stewart, 1981, p. 95). The network comprised one broadband seismometer (Romanowicz *et al.*, 2003) with a flat response from 2.8 mHz to 50 Hz

^{a)}Electronic mail: wilcock@u.washington.edu

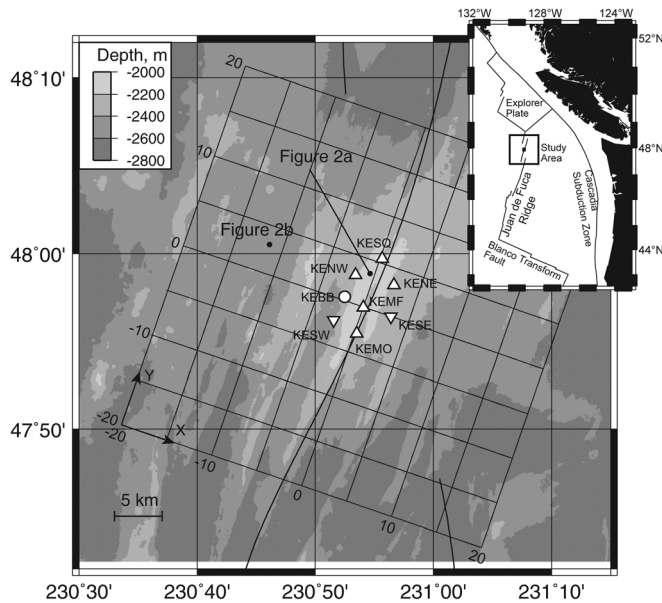


FIG. 1. Bathymetric map of the central Endeavour segment of the Juan de Fuca Ridge contoured at 200 m showing the seismic network (triangles for short period seismometers in coreholes, inverted triangles for short period seismometers in seismonuments and a circle for a broadband seismometer), the x-y grid used to locate whales (feint lines labeled in kilometers) and the location of plate boundaries (bold lines). Black dots show the locations of the two calls shown in Fig. 2. The inset figure shows the location of the experiment area relative to the Pacific Northwest and tectonic plate boundaries.

that was sampled at either 50 or 100 Hz and seven short period seismometers (Stakes *et al.*, 1998) with a reasonably flat response from 1–90 Hz that were sampled at 128 Hz. The network is similar in layout and instrument characteristics to other small aperture seafloor networks except that the instruments were deployed below the seafloor with a remotely operated vehicle, rather than by free-falling from a research vessel. The broadband seismometer was buried in sediments, five of the short periods were inserted into horizontal coreholes drilled into basalt and the remaining two were placed in concrete seismonuments that were partially buried in sediments (Wilcock *et al.*, 2007). Each seismometer was located with an accuracy of ~ 10 m using an ultra-short baseline navigation system on the remotely operated vehicle. The instruments recorded autonomously for 1 year and were redeployed twice to collect 3 years of data.

The 20-Hz vocalization of fin whales has been described by many researchers (Schevill *et al.*, 1964; Watkins *et al.*, 1987; Thompson *et al.*, 1992; McDonald *et al.*, 1995). The vocalization is a down-swept pulse lasting ~ 1 s, most commonly in the frequency range of 18–23 Hz (Watkins *et al.*, 1987). Call sequences may last more than 1 day and often occur at regular intervals. At the Endeavour, the calls are highly seasonal with the highest density of calls observed from November to early March and very few from May to August (Soule *et al.*, 2009). The data set contains $\sim 300\,000$ fin whale calls and several hundred tracks. For a call within or very close to the network [Fig. 2(a)], each OBS will typically record the direct arrival and up to two multipath arrivals. For calls outside the network [Fig. 2(b)], the signal to noise is lower but four or more multipath arrivals are often

visible because seafloor reflection coefficients increase with incidence angle.

III. WHALE DETECTION AND ARRIVAL TIME DETERMINATION

The identification and classification of biological sounds in large datasets is a topic of considerable research and several studies have evaluated sophisticated methods for fin whales (e.g., Mellinger and Clark, 1997; Muoy *et al.*, 2009). A simple method was employed in this study since the fin whale calls are abundant and tracking is not dependent on detecting every call in a sequence. As is common for marine microearthquake studies (Lee and Stewart, 1981, pp. 52–55), the ratio of the root mean squared (RMS) average in running short- and long-term windows is used to trigger on impulsive arrivals. A trigger threshold ratio of 3 and window lengths of 0.25 and 60 s are used after applying a 10–35 Hz band-pass filter. Triggers are grouped into an event when they are detected on at least eight channels and four stations within a 2.5 s interval. The term “event” is used to describe a signal that is potentially locatable because it is recorded on several stations.

Since microearthquakes have the majority of their energy below 10 Hz (e.g., Aki, 1967) while fin whale calls are centered near 20 Hz, the spectra of the ground velocity recorded by the seismometers can be used to discriminate between whales and earthquakes. If the spectral energy within a frequency band extending from 15–35 Hz exceeds that within a 5–15 Hz band for a majority of the triggers in an event, the event is classified as a fin whale call.

The automatic algorithm used to identify arrival times is illustrated in Fig. 3. The instantaneous amplitude and frequency are calculated for each record using the Hilbert transform (Bracewell, 1978) and a noise level is defined as the median absolute amplitude in a 20-s window centered on the trigger. The instantaneous amplitude is zeroed for samples where the instantaneous frequency is < 15 Hz [Fig. 3(b)] and also during instrumental noise spikes that occur in the data each minute and during disk writes every 20 min. The instantaneous amplitudes are weighted with the reciprocal of the squared noise level and summed for the three seismometer channels. The amplitude is then smoothed with a cosine taper with a half width of 0.2 s to yield an amplitude envelope function whose noise level is defined as the median value [Fig. 3(c)].

To identify potential arrivals, all the maxima in the function that exceed the noise level by a factor of 2 are selected. The term “arrival” is used to refer to a recording of a fin whale call that has propagated either along a direct path or a multipath that includes one or more pairs of reflections from the seafloor and sea surface. Because the 20-s window can in some instances include arrivals from more than one call, maxima more than 2 s before the earliest trigger time in an event are discarded. Maxima are also eliminated if there is a higher amplitude maxima within 1 s (since the spacing of multipaths always exceeds this for the ranges and water depths encountered in this study). In a flat-bottomed setting, the time between successive multipath arrivals increases

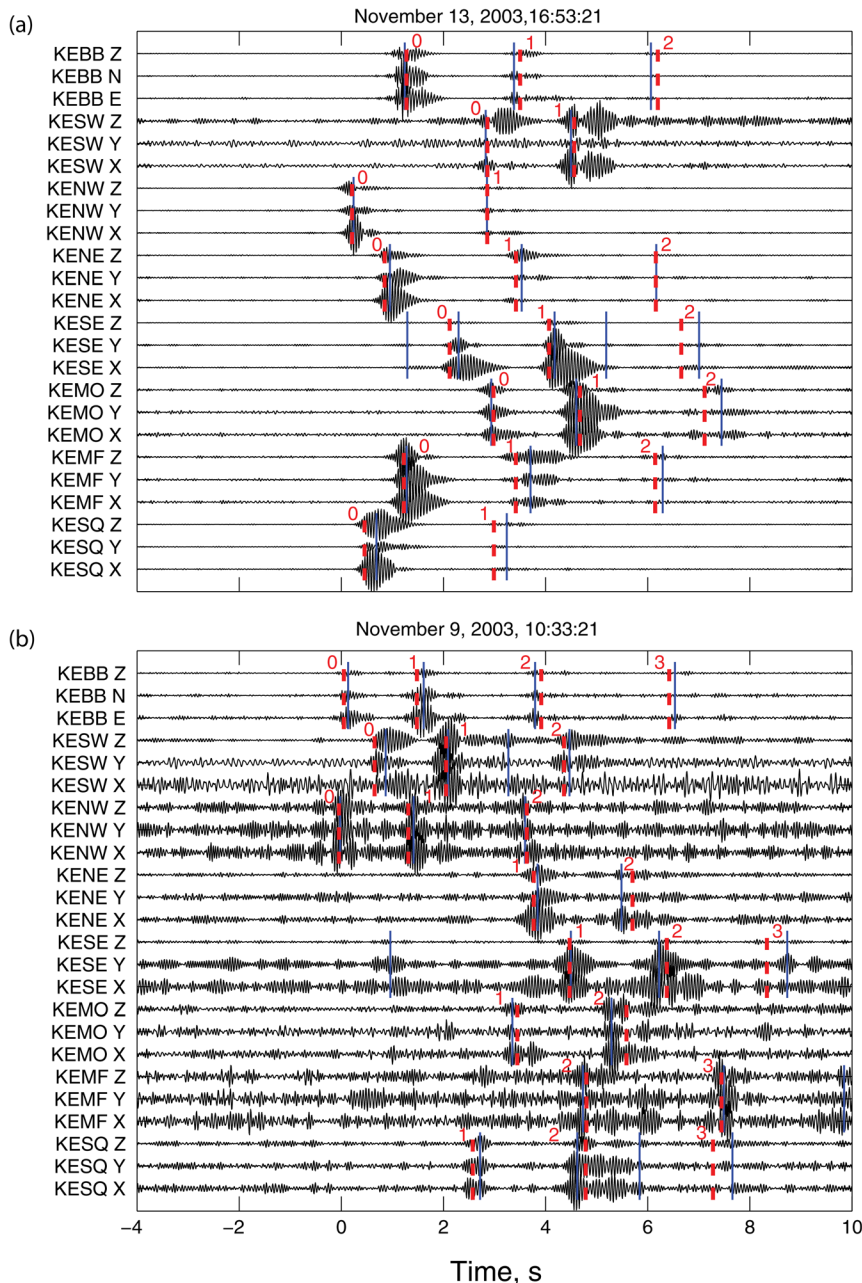


FIG. 2. (Color online) Seismic records for (a) a fin whale within the seismic network and (b) a fin whale about 10km to the west of the network (Fig. 1). Each figure shows traces for the vertical (labeled with the station name and Z) and two horizontal channels (labeled with the station name and X and Y) for all eight seismometers. Times are relative to the first arrival and the amplitudes on each seismometer are normalized to the maximum amplitude recorded on the three channels. Solid vertical lines show the picked arrival times and bold dashed lines show the predicted times labeled with the number of water column multiples assumed for the predictions. The traces have been filtered with a 5 Hz high-pass filter.

[Fig. 4(a)]; times that do not satisfy this relationship are also eliminated subject to a jitter of 0.2s to allow for variable seafloor depths.

For each arrival the start and end time are found by determining when the amplitude rises a factor of 1.5 above the noise level. For purposes of locating the whale, the start times are unreliable because the calls are emergent and the time identified thus dependent on the overall signal to noise. Two alternative means of picking the arrival time were evaluated: the time of the maximum amplitude and the mid-energy point. Since both approaches lead to locations with similar travel time misfits, the simpler approach of picking times at the maximum amplitude is adopted. For each arrival time, a crude estimate of the uncertainty is obtained by calculating the half width of the interval in which amplitudes exceed half the maximum value. When the signal to noise, x_{sn} , is less than 5, this uncertainty is then multiplied by a factor of $(2.25 - 0.25 x_{sn})$

IV. LOCATIONS BASED ON ARRIVAL TIMES

Locating biological sounds in the ocean with widely spaced receivers is a long standing problem (Walker, 1963; Speisberger and Fristrup, 1990) and the topic of extensive literature. For networks of near-bottom receivers, efforts have been made to develop and evaluate techniques using data from Navy test ranges (e.g., Tiemann *et al.*, 2004; Morrissey *et al.*, 2006; Nosal and Frazer, 2006; 2007; Baggenstoss, 2011). The most commonly used methods are based on using the time-difference between arrivals at different stations (Speisberger and Fristrup, 1990; Morrissey *et al.*, 2006; Baggenstoss, 2011); other methods make use of sea-surface or seafloor reflected arrivals (Nosal and Frazer, 2006) or apply computationally intensive techniques that require no assumptions about the path by which energy travels to the receiver (Nosal and Frazer, 2007). The objective of the location algorithm presented here is to provide a computationally efficient

November 13, 2003, 16:53:21 Station KESW

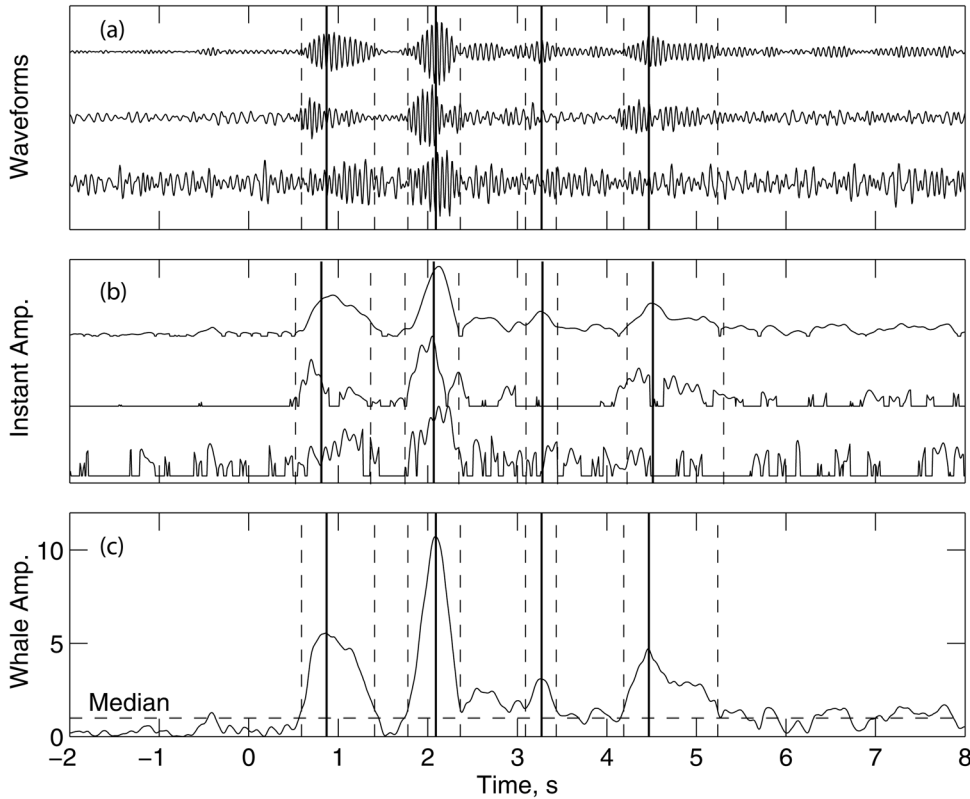


FIG. 3. Examples of automated arrival times for station KESW. (a) Waveforms for each channel filtered with a 5 Hz high-pass filter and plotted with equal maximum amplitudes. (b) Instantaneous amplitude normalized to the maximum value for each channel with the values zeroed when the instantaneous frequency falls below 15 Hz. (c) A fin whale amplitude function derived by summing the instantaneous amplitudes after weighting by the reciprocal of the squared noise level, smoothing with a cosine taper with a half width of 0.2 s, and normalizing by the median value. The times of the maximum amplitude and the onset and end times of the arrivals are shown by the solid and dashed lines, respectively.

method to find the call location that best fits a set of arrival times without *a priori* information about the path of the arrivals and in the potential presence of a few bad arrival times. A grid search method is used because it provides a systematic method to evaluate different locations and assumptions about arrival paths.

The grid (Fig. 1) measures 40 km \times 40 km with an initial grid spacing of 0.5 km and is centered on the seismic network and aligned with the ridge axis. Because fin whale calls are

believed to be generated at fairly shallow depths (Watkins *et al.*, 1987) and each recorded arrival will be the sum of the direct path and downward reflection from the seafloor, the calls are assumed to be located on the sea surface for simplicity. Travel times are calculated for direct and multipath arrivals from points on the grid to the ocean bottom seismometers using the RAY two-dimensional ray tracing software (Bowlin *et al.*, 1993) and a water velocity profile (Fig. 5) derived from a global database (Levitus, 1982). The RAY software can accommodate an arbitrary bathymetry along a profile but in the presence of rough bathymetry it is in some instances difficult to find an eigenray for multipaths while in others several eigenrays are found. To compute unique travel times efficiently, direct paths are first calculated for various water

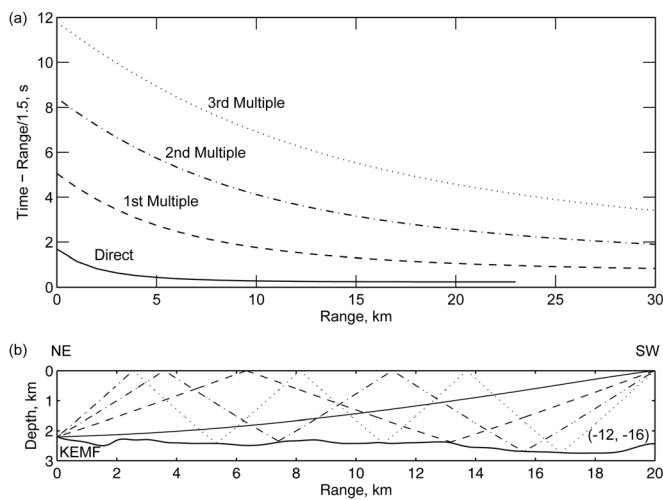


FIG. 4. (a) Predicted travel times plotted as a function of range for the direct arrival (solid) and 1st (dashed), 2nd (dot-dashed), and 3rd (dotted) multipaths assuming a constant water depth of 2500 m. (b) Examples of ray paths computed for the direct arrival (solid) and 1st (dashed), 2nd (dot-dashed), and 3rd (dotted) multipaths for a source located 20 km away from station KEMF at $x = -12$ km and $y = -16$ km.

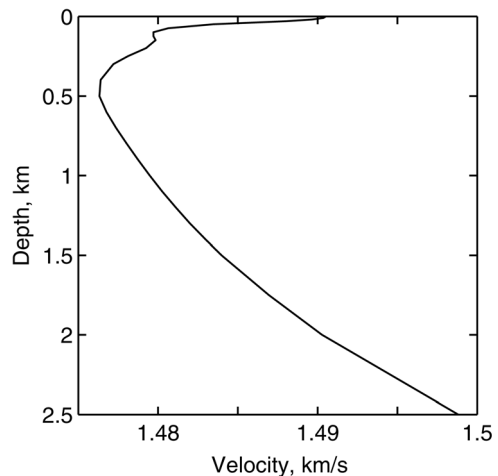


FIG. 5. Vertical water velocity model used to trace rays (Levitus, 1982).

depths and ranges. These are then pieced together to create multipaths in an iterative process that adjusts path segments to match the seafloor depth at bottom bounce points while maintaining a constant ray parameter. The resulting paths [Fig. 4(b)] are equivalent to those obtained from a full calculation except that the seafloor is assumed to be horizontal at the bounce points.

For the grid search, six different assumptions about the arrival path of one arrival are considered. Three arrival times on different stations are selected by finding the largest amplitude arrival on each station and choosing the three earliest. Each of these arrivals is assumed in turn to be a direct and first multipath arrival. For a given grid point and assumption about the path of one arrival, the origin time T_O can be estimated by

$$T_O^{\text{pred}}(\mathbf{x}, h) = T_g^{\text{obs}} - t_g^{\text{pred}}(\mathbf{x}, h), \quad (1)$$

where T^{obs} is the observed arrival time of the selected arrival, t^{pred} the predicted travel time, \mathbf{x} the horizontal spatial position of the grid point, g the index of the arrival time, and h the index of the six path assumptions. This estimate of the origin time allows the arrival times of all paths to the grid point from each station to be predicted. Each observed arrival time is then matched to a path by finding the predicted arrival time that most closely matches its time. If two arrival times on one station are modeled by the same path, the arrival time with the larger absolute misfit (where misfit is defined as the difference between the observed and predicted arrival times) is assigned as unmodeled. Arrival times with absolute misfits of greater than five times the median value for the call are also assigned as unmodeled. The predicted origin time is recalculated using the modeled arrival times according to

$$T_O^{\text{pred}}(\mathbf{x}, h) = \frac{\sum_{g=1}^{m(\mathbf{x}, h)} (T_g^{\text{obs}} - t_g^{\text{pred}}(\mathbf{x}, h)) / \sigma_g^2}{\sum_{g=1}^{m(\mathbf{x}, h)} 1 / \sigma_g^2}, \quad (2)$$

where m is the number of modeled arrival times and σ the arrival time uncertainty estimated when the arrival times were determined (see Sec. III). The normalized root mean squared travel time residual, r is then calculated according to

$$r(\mathbf{x}, h) = \sqrt{\frac{1}{m(\mathbf{x}, h)} \sum_{g=1}^{m(\mathbf{x}, h)} \frac{(t_g^{\text{obs}}(\mathbf{x}, h) - t_g^{\text{pred}}(\mathbf{x}, h))^2}{\sigma_g^2}}, \quad (3)$$

where the observed travel time, t_g^{obs} is given by

$$t_g^{\text{obs}}(\mathbf{x}, h) = T_g^{\text{obs}} - T_O^{\text{pred}}(\mathbf{x}, h). \quad (4)$$

The optimal solution is the grid point and arrival path assumption that simultaneously maximizes the number of modeled arrivals $m(\mathbf{x}, h)$ and minimizes the normalized residual $r(\mathbf{x}, h)$. These two quantities need to be optimized together. In the

presence of bad arrival times, a solution that maximizes just the number of modeled arrival times may be spurious. For example, a bad arrival time that is early (e.g., station KESE in Fig. 2) might be fit by a direct path with other arrivals fit by paths with too many water column multiples. A solution that minimizes only the residual may have an unacceptably small number of modeled arrival times.

The approach used in this study is to sort $m(\mathbf{x}, h)$ and find the value that corresponds to the 90th percentile, m_{90} . The grid search process is then repeated with the modification that solutions with $m(\mathbf{x}, h) < m_{90}$ are rejected and all other solutions are calculated based on the best-fitting m_{90} arrival times. The minimum value of $r(\mathbf{x}, h)$ is used to determine the set of modeled arrival times and their paths. Since the set of modeled arrival times and their assumed paths may differ between grid points, the grid search is repeated for a final time assuming the same set of modeled arrival times and paths at all grid points. This leads to a smooth residual function $r(\mathbf{x})$ with a single minimum. A more precise solution can be obtained either by using a finer grid locally around the minimum or by using a cubic spline to interpolate $r(\mathbf{x})$ to a finer grid. Comparisons of the two methods show that solutions found by interpolation lie within less than a tenth of the initial grid spacing (i.e., < 50 m) of the solutions found with a finer grid.

Following the procedure used for earthquake studies (e.g., Wilcock and Toomey, 1991) the spatial uncertainty of the solution can be estimated from confidence levels in the spatial residual function $r(\mathbf{x})$ that are derived from the F -statistic according to

$$r_{1-\alpha}^2(\mathbf{x}) = \min[r^2(\mathbf{x})] + \frac{(p-1)}{m} s^2 F(p-1, M, 1-\alpha), \quad (5)$$

where $1-\alpha$ is the confidence level, s is the arrival time uncertainty and $p=3$ is the number of free parameters in the solution (origin time and two horizontal coordinates) with the term $(p-1)$ appearing in the equation because uncertainties in call origin time are generally of little interest. If the absolute values of the arrival time uncertainties are correct then s should be unity, but if the arrival time uncertainties are only relative, s can be estimated according to

$$s^2 = \frac{\sum_{i=1}^n \frac{m_i^2}{m_i - p} \min[r_i^2(\mathbf{x})]}{M}, \quad (6)$$

with r_i and m_i are the residual and number of modeled arrival times for the i^{th} of n calls and M given by

$$M = \sum_{i=1}^n m_i - p. \quad (7)$$

Since M is large for the data set used in this study, the F -statistic can be replaced by the chi-squared statistic. To avoid small uncertainty levels for solutions with large residuals, s^2 can be replaced with the RMS arrival time residual for the

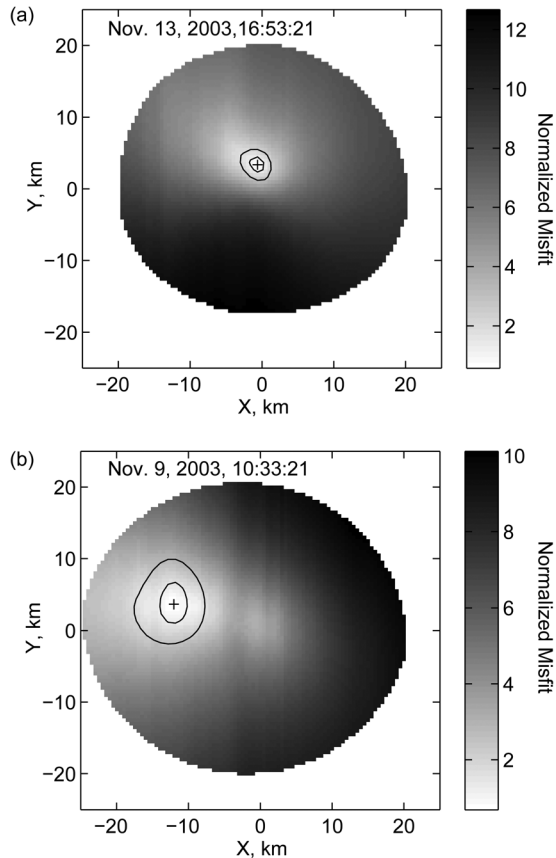


FIG. 6. Examples of the locations for the events shown in (a) Fig. 2(a) and (b) Fig. 2(b). The shading shows the root-mean-squared normalized misfit with the location of the minimum values shown by pluses. Solid lines show contours at the approximate $1-\sigma$ and $2-\sigma$ uncertainty levels.

particular solution when it is larger than s^2 . This yields uncertainty levels of

$$r_{1-\alpha}^2(\mathbf{x}) = \min[r^2(\mathbf{x})] + \frac{p-1}{m} \max\{s^2, \min[r^2(\mathbf{x})]\} \times \chi^2(p-1, 1-\alpha). \quad (8)$$

Figure 2 shows the predicted arrival times and modeled number of multipaths for two example calls, while Fig. 6

shows the location and uncertainty contours. For locations within the network the formal $1-\sigma$ uncertainties are ~ 0.5 km while outside the network they can reach several kilometers. A significant contribution to these uncertainties is the difficulty of identifying a single arrival time for each multipath when the waveform includes several local maxima [e.g., the 1st multipath for station KESW in Fig. 2(a) and the 2nd multipath for station KESQ in Fig. 2(b)]. This is likely the result of alternate paths for each multipath due to the complex bathymetry and suggests that uncertainties might be significantly smaller in regions of smooth bathymetry.

The location method works well for most tracks within and near the network but it is increasingly subject to mislocations as the distance outside the network exceeds 5 km; at larger distances there are more bad arrival times because of the lower signal to noise and the algorithm sometimes finds alternative locations at similar azimuths to the center of the network with all the arrivals fit by an additional water column multiple at the more distant location. To eliminate bad locations automatically a median filter with a 300-s window is applied to the x and y locations for sequence of calls. If the resulting track shows unreasonable jumps (more than three times the location uncertainty for adjacent calls) the track is discarded; if not then only those locations lying near the track are kept. When only one whale is calling near the network, this method generally allows tracks to be obtained up to ~ 15 km from the network center.

When several whales are calling along the same track or there are whales calling in more than one location, the calls often overlap. When the sets of arrival times used for the locations often include times for more than one call, the location method will find many spurious locations and median filtering methods may not find a feasible track. In such instances, analyst intervention can be used to identify the track(s) by inspecting the locations and the modeled and predicted arrival times for individual calls to identify those that appear to be from single calls. For the Endeavour data set, analyst intervention significantly increases the total duration of tracks.

Figure 7 shows examples of tracks determined using the automated method. In the first two tracks, a fin whale swims across the experiment region in 4–5 h at speeds of ~ 8 km/h.

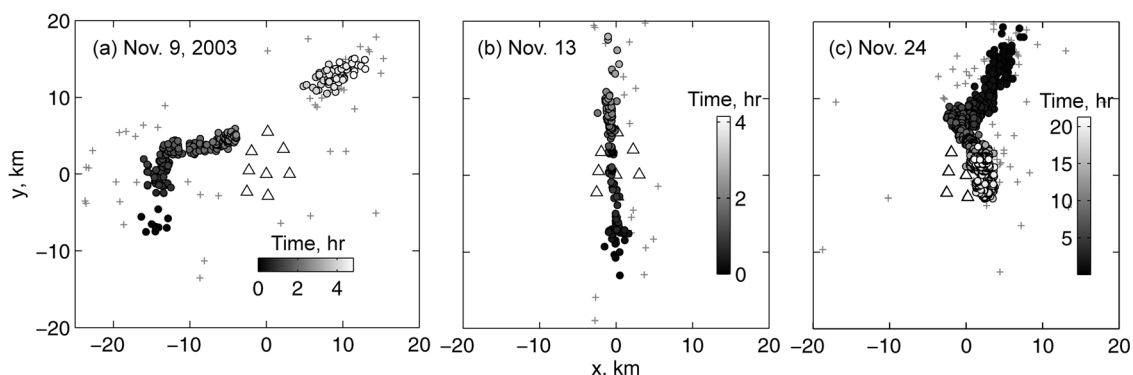


FIG. 7. Examples of fin whale tracks for (a) November 9, (b) November 13, and (c) November 24, 2004 with the location of individual calls shown by circles with shading indicating the time relative to the first call. Locations that have been rejected because they lie off the track (pluses) and the seismic network (open triangles) are also shown.

There are two long gaps in the call sequence of the first track and many shorter gaps in the second. The third track lasts over 20 h and is a meandering track with an overall north to south direction and a much slower net swimming speed.

V. ADDING ADDITIONAL CONSTRAINTS TO THE LOCATIONS

The usefulness of including additional constraints in the location from the amplitudes and particle motions of the arrivals was also investigated. Figure 8 shows the mean peak amplitude (in units of ground velocity measured by the seismometers) as a function of range for direct arrivals and 1st and 2nd multipaths for station KESQ and a data set of nearly 5000 arrivals in six tracks chosen to provide complete azimuthal coverage. At ranges ≤ 5 km the amplitudes of the paths are quite distinct. At 5 km and ~ 10 km the amplitude of the direct path decreases below those of the 1st multipath and 2nd multipath, respectively. At ranges above 10 km the amplitudes are of limited use in discriminating between paths because their variations overlap one another. The ratios of the amplitudes of the 1st multipath to the direct arrival and of the 2nd multipath to the 1st multipath (Fig. 9) show significant variations at a given range but are distinct from one another at ranges between about 4 and 11 km. Thus, for this experiment the amplitude data is not particularly useful for constraining distances when the calls are located much greater than 10 km from the source.

Three component OBSs measure the orientation of the ground motion and thus potentially constrain the azimuth and incidence angle (or range) of the source. At the seafloor the incoming compressional wave is partially reflected back into the water column and partially transmitted downward as *P* and *S* waves. The OBS measures the combined motions of the transmitted *P* and *S* waves. Figure 10 shows the apparent

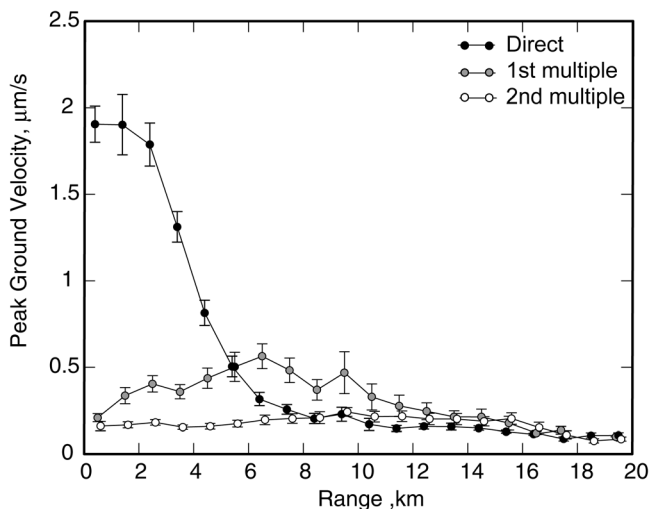


FIG. 8. Mean of the observed peak ground velocity versus range for the direct (black circles), 1st water-path multiple (grey circles) and 2nd water path multiple (white circles) for station KESQ. The circles show the mean value in 1-km range increments and the error bars show their standard deviation. The plot is based on 4875 located fin whale calls observed on August 25, November 9, November 13, and November 24, 2003 and January 14 and February 3, 2004.

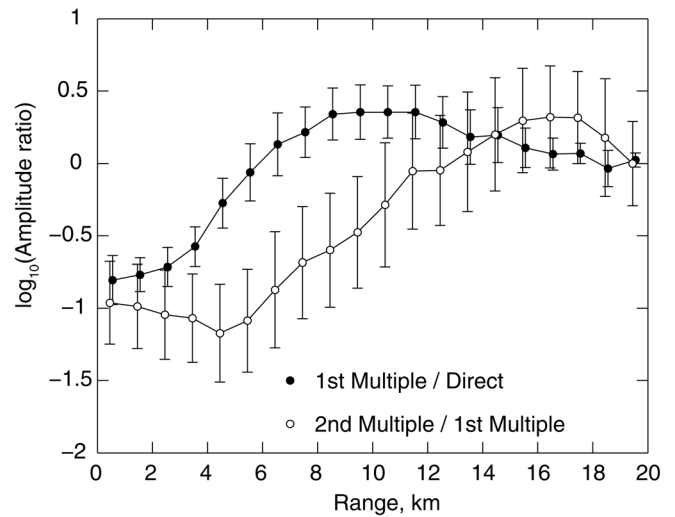


FIG. 9. Observed mean ratios of the amplitude of the 1st water path multiple to the direct arrival (black circles) and the 2nd water path multiple to the 1st water path multiple (white circles). The circles show the mean value in 1-km range increments and the error bars show their standard deviation. The plot is based on the same located calls as Fig. 8 but includes data for all OBSs.

incidence angle as a function of range for a 2.5-km-deep ocean for two sets of seafloor models, one for a basaltic basement and the other for sediments, calculated using the Zoeppritz equations for a liquid-solid interface (Ikelle and Amundsen, 2005). At the critical angle, which occurs at about ~ 2 km range in the basalt model and ~ 4 km in the sediment model, the particle motions are horizontal and at ranges beyond the critical angle they remain nearly so. For the basalt model [Fig. 10(a)], the incidence angle can exceed 90° for higher *S*-wave velocities. This suggests that at all but the shortest ranges the particle motions only constrain azimuth with a 180° ambiguity and do not constrain range. Analysis of the particle motions for our data set confirms that this is the case.

Figure 11 shows two examples of the mean misfit between the located azimuth and the azimuth determined from the first principal component of the particle motions (with the 180° ambiguity removed) plotted against the located azimuth. The data show a significant amount of scatter suggesting that the azimuths determined from the particle motions have errors up to tens of degrees for the short period sensors [Fig. 11(a)] and about 10° for the broadband sensor [Fig. 11(b)]. These errors are presumably a result of location errors, out-of-plane propagation and scattering in the rough topography, and possibly poor coupling of the short period sensor. Given the inherent 180° ambiguity and the scatter in values, particle motions provide only limited constraints on the location for this experiment.

VI. CROSS-CORRELATION AND DOUBLE-DIFFERENCE LOCATIONS

The uncertainties associated with the call locations obtained by the location method are quite large (Fig. 6). This limits their utility for analyzing fine-scale swimming

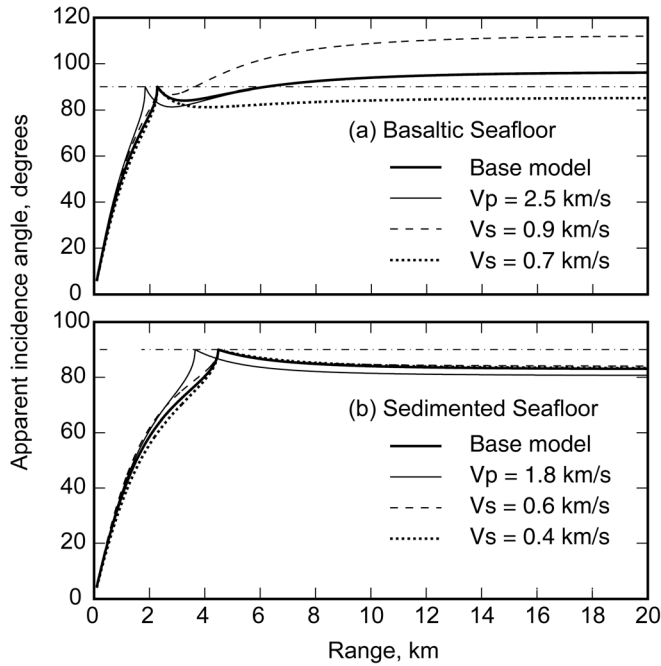


FIG. 10. (a) Apparent incidence angle (particle motions) observed for a direct arrival versus range for a base model parameters that are appropriate for young basaltic seafloor (bold black line) (Christeson *et al.*, 1994; Gilbert and Johnson, 1999)—a sound wave velocity in water $V_W = 1.5 \text{ km s}^{-1}$, a water density $\rho_W = 1030 \text{ kg m}^{-3}$, a crustal P -wave velocity $V_P = 2.2 \text{ km s}^{-1}$, a crustal S -wave velocity $V_S = 0.8 \text{ km s}^{-1}$, and a crustal density $\rho_C = 2200 \text{ kg m}^{-3}$. Also shown are curves for the same parameters except that V_P is changed to 2.5 km s^{-1} (faint solid line) and V_S is changed to 0.9 km s^{-1} (dashed line) and 0.7 km s^{-1} (dotted line). (b) As for (a) except the seafloor properties for the base model are for sediments (Sun, 2000)— $V_P = 1.7 \text{ km s}^{-1}$, $V_S = 0.5 \text{ km s}^{-1}$, and $\rho_C = 1700 \text{ kg m}^{-3}$ and curves are shown for changing V_P to 1.8 km s^{-1} and V_S to 0.6 and 0.4 km s^{-1} .

patterns and determining swimming speeds that take into account meandering paths. The location errors arise from two sources: errors in the arrival times (clock errors, arrival time identification) and errors in the travel time calculations (water column velocity structure, bathymetry, simplifying assumptions in ray path calculations). When comparing the location of adjacent calls the scatter arises from those components of the error that are unsystematic. For the arrival times along a given track, clock errors will be systematic but the errors in automatic arrival time identification may not be. For the travel time calculations, the errors arising from arrival times for paths that are common for the two calls will be systematic but the errors for arrival times that are only available for one call will contribute to the scatter.

In seismology, waveform cross-correlation is a commonly used technique to ensure that the observed arrival times are consistent for nearby events with similar waveforms (e.g., VanDecar and Crosson, 1990; Schaff *et al.*, 2004). The raw fin whale calls are not suited for cross-correlation because the frequency sometimes varies between calls, and cross-correlation may misalign the calls by a full cycle (0.05 s for a 20 Hz call) because the frequency is only gently downsweped. However, cross-correlation works well on the amplitude envelope function (Fig. 12). The envelope function is often characterized by several local maxima [e.g., Fig. 12(b)], a result presumably of interference between arrivals taking slightly

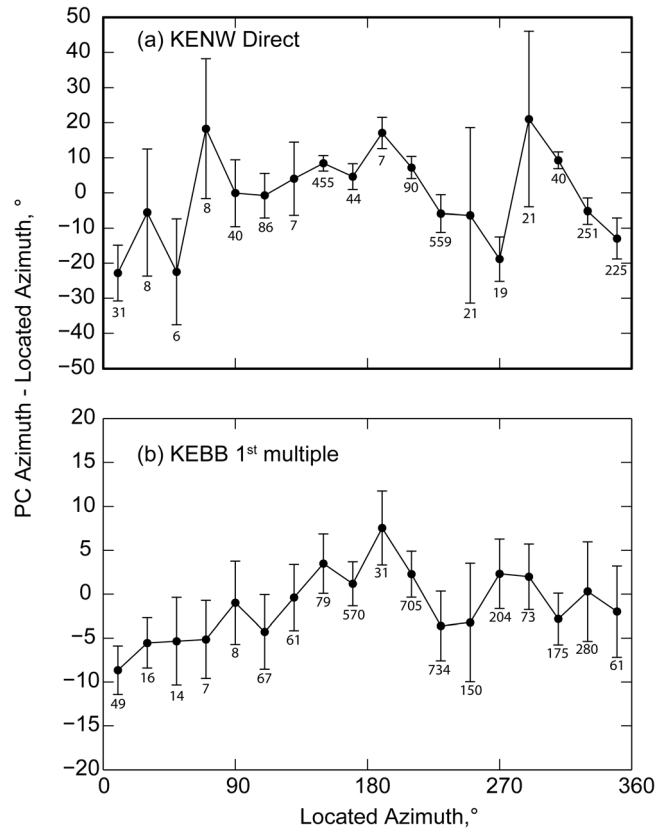


FIG. 11. (a) Observed difference and standard deviation between the arrival azimuth for the whale location and that inferred from particle motions (corrected for a 180° ambiguity) as a function of azimuth for the direct arrival to station KENW. Filled circles show the mean values in 20° bins, error bars show the standard deviation and labels the number of observation in each bin. (b) As for (a) except for the 1st multiple to station KEBB.

different paths and scattered energy. The shape of the amplitude envelope function is generally very similar for nearby calls. Cross-correlation can be used to determine an arrival time correction that makes times consistent.

The double-difference method (Waldhauser and Ellsworth, 2000) is a relatively new technique in seismology that has been developed to reduce scatter in locations of nearby earthquakes. Instead of seeking to minimize the residuals between observed and predicted arrival times, the method considers pairs of events recorded at a common station and seeks to minimize the difference in residual d

$$d_{k,l,i,j} = (T_{k,l,i}^{\text{obs}} - T_{k,l,j}^{\text{obs}}) - (T_{k,l,i}^{\text{pred}} - T_{k,l,j}^{\text{pred}}), \quad (9)$$

where the index k indicates the station, l the arrival path, and i and j the events. These double-difference times can be computed for automatic and cross-correlation arrival times. For nearby events they will minimize systematic errors in travel time predictions because the paths are very similar. If cross-correlation arrival times are used they will also minimize the systematic errors arising from inconsistencies in identifying arrival times.

Given initial estimates of call locations, each double-difference time can be equated to changes in call locations assuming linearity according to

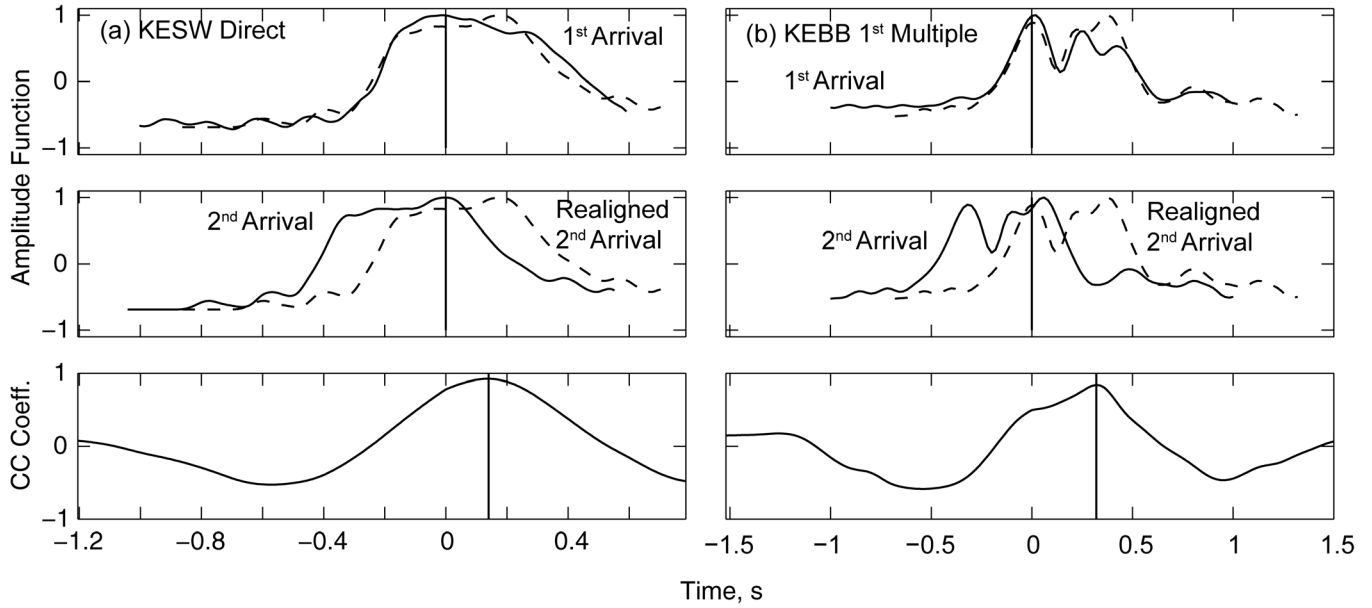


FIG. 12. (a) Example of the cross-correlation of the whale amplitude function for direct arrivals recorded by station KESW for two nearby calls. The upper panel shows the demeaned whale amplitude function for the 1st call (solid line) and the realigned 2nd call (dashed line). The middle panel shows the normalized whale amplitude function for the 2nd call solid before (solid) and after (dashed) realignment. The lower panel shows the cross-correlation function. The maximum value (vertical line) provides a correction to the differential travel time. (b) As for (a) except the whale amplitude functions are for a 1st water path multiple recorded by station KEBB.

$$\begin{aligned} \frac{\partial t_{k,l,i}}{\partial x} \Delta x_i + \frac{\partial t_{k,l,i}}{\partial y} \Delta y_i + \Delta T_{O,i} - \frac{\partial t_{k,l,j}}{\partial x} \Delta x_j \\ - \frac{\partial t_{k,l,j}}{\partial y} \Delta y_j - \Delta T_{O,j} = d_{k,l,ij}, \end{aligned} \quad (10)$$

where t is the predicted travel time, Δx , Δy , and ΔT_O are changes in the x coordinate, y coordinate, and origin time, respectively. For a set of double-difference times, Eq. (10) yields a matrix equation of the form

$$\mathbf{Gm} = \mathbf{d}, \quad (11)$$

where \mathbf{G} is a sparse matrix of partial derivatives, \mathbf{m} is vector of changes in call positions and origin times, and \mathbf{d} is a vector of double-difference times. If the uncertainties of the double-difference times differ the rows of Eq. (11) can be weighted by the reciprocal of the uncertainty. Additional equations can be added to Eq. (11) to set the mean adjustment in each location parameter to zero

$$\begin{aligned} \sum_{i=1}^N \Delta x_i &= 0, \\ \sum_{i=1}^N \Delta y_i &= 0, \\ \sum_{i=1}^N \Delta T_{O,i} &= 0, \end{aligned} \quad (12)$$

where N is the number of calls.

To stabilize the solution of Eq. (11), damping equations can also be added to limit changes in unresolved model parameters yielding

$$\begin{bmatrix} \mathbf{G} \\ \lambda \mathbf{I} \end{bmatrix} \mathbf{m} = \begin{bmatrix} \mathbf{d} \\ 0 \end{bmatrix}, \quad (13)$$

where λ is a damping weight and \mathbf{I} the identity matrix. Since the number of double-difference times will be large for even quite a small set of calls, Eq. (13) can be minimized in a least-squares sense using the LSQR technique (Paige and Saunders, 1982). To account for non-linearity and eliminate spurious difference times, an iterative solution scheme is employed. After each iteration, the difference times are recalculated and those with absolute values exceeding a threshold set to a multiple of the median absolute misfit are removed. Equation (13) is solved again with the new difference times and the process repeated until the solution converges.

Figure 13 shows segments of the fin whale tracks from Fig. 7 that have been recomputed using the double-difference technique with automatic arrival times and with cross-correlation arrival times. Cross-correlation arrival times are only included when the correlation coefficient exceeds 0.7. The double-difference technique requires that the distance between two calls is small compared with the distance to the station. For a regional seismic network with stations up to 200 km from the earthquake cluster, Waldhauser and Ellesworth (2000) limit double-difference times to earthquake pairs that are < 10 km apart. The network in this study is substantially smaller; double-difference times for the solutions shown in Fig. 7 were limited to calls within 300 s of each other (equivalent to a call spacing of ~ 300 m at a typical swimming speed of 4 km/h). Including calls up to 1 km apart has little impact on the solutions for tracks outside the network but increases the scatter of the locations

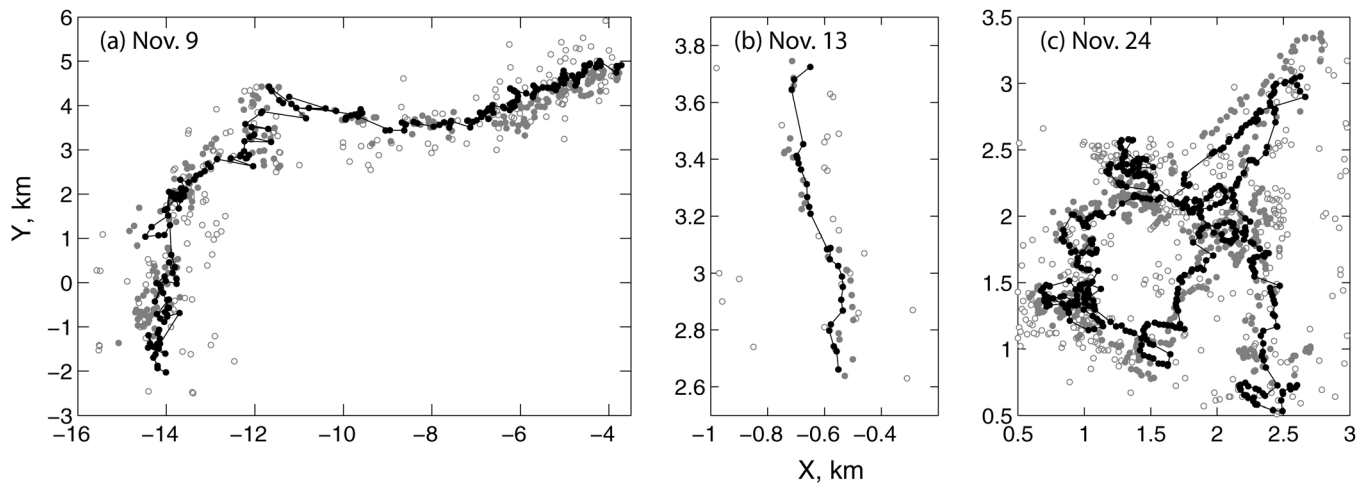


FIG. 13. Comparison of tracks obtained by locating whales with the grid search method (open circles), the double-difference method using automated arrival times (gray circles), and the double-difference method using cross-correlated arrival times (connected black circles) for segments of fin whale tracks from Fig. 7. (a) On November 9, 2003 the initial track segment contains 213 calls that were located with an RMS travel time misfit of 0.25 s. A total of 16 535 and 11 592 double-difference times from the automatic arrival times and cross-correlation were inverted separately to yield tracks with RMS residuals for the double-difference times of 0.085 and 0.038 s, respectively. (b) On November 13, 2003 the initial track segment contains 25 calls that were located with an RMS travel time misfit of 0.25 s. A total of 1362 and 1287 double-difference times from the automatic arrival times and cross-correlation were inverted separately to yield tracks with RMS residuals for the double-difference times of 0.028 and 0.017 s, respectively. (c) On November 24, 2003 the initial track segment contains 423 calls that were located with an RMS travel time misfit of 0.26 s. A total of 27825 and 23988 double-difference times from the automatic arrival times and cross-correlation were inverted separately to yield tracks with RMS residuals for the double-difference times of 0.035 and 0.017 s, respectively.

and the travel time misfit within the network. It should be noted that where there is a significant gap between calling along a track [e.g., Fig. 7(a)], the segments of the track will not be linked by double-difference times and so are relocated independently (Waldhauser and Ellesworth, 2000).

For large data sets, the inclusion of all the difference times leads to a very large number of equations and a lot of redundancy; following the suggestion of Waldhauser (2001) the solutions in Fig. 13 were obtained by only including equations that link each call to a maximum of the ten nearest neighbors with at least eight double-difference times in common. Including more difference times has little effect on the solution but increases the computation time. The solutions in

Fig. 13 are based on 10 iterations. After each of the first five iterations, the threshold for eliminating double-difference times is set to six times the median value absolute misfit. This threshold is reduced to four times the median absolute misfit for the final five iterations. Five iterations at each threshold are sufficient to ensure that the solutions converge.

The first track [Fig. 13(a)] lies well outside the network and while there is a substantial reduction in the scatter of the calls, there are still significant errors at larger ranges with successive calls up to about a kilometer apart. The second and third track lines lie within the network and the double-difference locations lead to a significant improvement in the quality of the track. For the double-difference with cross-

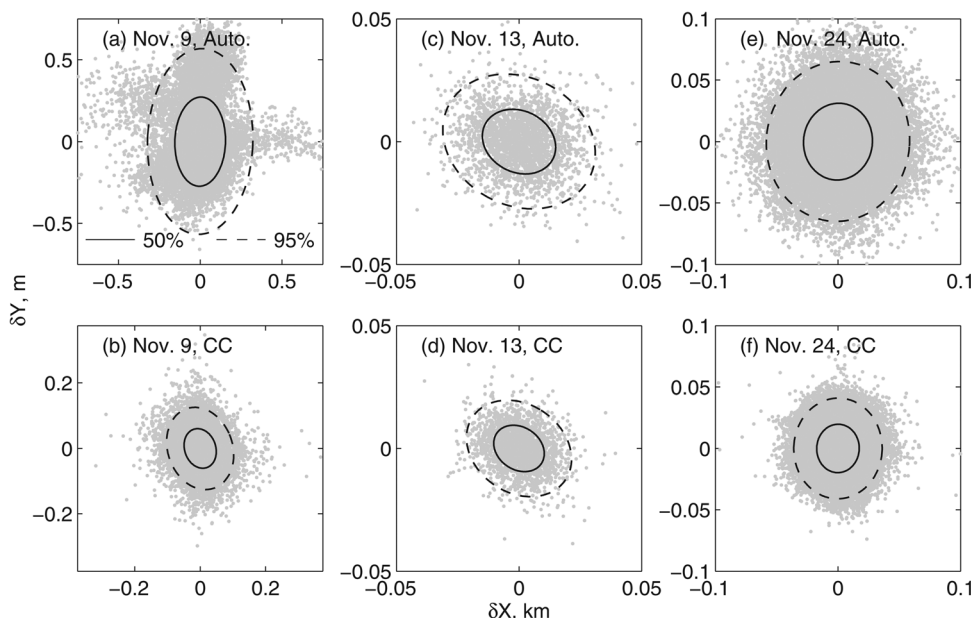


FIG. 14. Bootstrap analysis of the relative location error for the relocated tracks shown in Fig. 13. Each plot shows the a scatter plot (light gray circles) of the change in locations (δX , δY) obtained by repeating the double-difference inversion one hundred times with random errors added to double-difference times based on the observed distribution of misfits. The 50% (solid line) and 90% (dashed line) confidence ellipses are obtained from the covariance. Results are shown for the track of November 9 with difference times based on (a) automatic (labeled "Auto.") arrival times and (b) cross-correlation (labeled "CC"). (c),(d) As for (a),(b) except for the track of November 13. (e),(f) As for (a),(b) except for the track of November 24.

TABLE I. Bootstrap and jackknife location errors. Bootstrap errors are found by calculating the covariance of the change in locations obtained by repeatedly assigning random errors to observed difference times based on the observed distribution of difference time misfits. Jackknife errors are found by eliminating each station and call in turn from the solution and finding the median and maximum standard deviation of the change in location (Waldhauser and Ellesworth, 2000).

	November 9		November 13		November 24	
	Automatic	Cross-correlation	Automatic	Cross-correlation	Automatic	Cross-correlation
<i>Bootstrap Errors</i>						
Maximum, m	230	53	13	9	26	17
Azimuth of Maximum, °	2	161	117	125	6	2
Minimum, m	132	40	10	7	24	15
<i>Station Jackknife Errors</i>						
Median, m	66	39	12	9	31	19
Maximum, m	250	160	37	20	180	55
<i>Call Jackknife Errors</i>						
Median, m	8.2	3.9	1.4	0.9	0.2	0.4
Maximum, m	59	15	2.7	1.7	4.9	5.3

correlation arrival times, the track lines form a single well-defined path; larger spaces between successive located calls correspond to large time gaps between calls.

The estimates of the solution error provided by LSQR are unreliable (Paige and Saunders, 1982). Waldhauser and Ellesworth (2000) describe statistical resampling techniques to estimate errors. In the bootstrap method (Waldhauser and Ellesworth, 2000), the final residuals are replaced by values that are randomly drawn from the observed residual distribution and the events relocated with these residuals. The process is repeated many times to statistically sample the resulting change in location. Figure 14 shows scatter plots of the change in locations obtained from 100 repetitions together with 50 and 95 % confidence limits determined from the covariance (the errors are listed Table I). For the first track that lies outside the network, the errors are quite large when the automatic arrival times are used and not normally distributed [Fig. 14(a)], suggesting that the inversion includes some bad difference times. The errors for tracks based on cross-correlation difference times are 50 m for the track outside the network [Fig. 14(b)] and 10–20 m within the network [Figs. 14(d), 14(f)]. It is important to note that (1) these are estimates of relative location error for adjacent call and not the absolute location error and (2) the bootstrap method only assesses the non-systematic part of this relative error. An alternative means to assess the error is to look at the tracks themselves. Within the network many segments of the tracks with calls spaced 30–40 m apart do not double back on themselves [Fig. 13(b) and 13(c)] suggesting that the bootstrap error estimates are reasonable.

Another means to assess errors is the jackknife method (Waldhauser and Ellsworth, 2000), which involves systematically eliminating data from one station or one call from the relocation. The standard deviation of the absolute change in location is measured for each call and the median and maximum values determined (Table I). The median jackknife errors for eliminating stations are similar to the errors obtained by the bootstrap method; because there are only

eight stations each station contributes significantly to the solution. The jackknife errors for eliminating calls are very small which indicates that each call is well connected by double-difference times to many others and thus not sensitive to the elimination of one call.

VII. CONCLUSIONS

This paper has presented a method for locating fin whale calls with an OBS network and demonstrates the practicality of using a network of closely spaced OBSs to track fin whales up to ~15 km from the network. The time-domain method to identify arrival times is based on the instantaneous frequency and amplitude envelope and is fairly specific to fin whales. However, the grid search location technique might be applicable to other marine mammal calls or anthropogenic sounds provided that (1) the sound source is sufficiently short and the water depth is sufficiently large that the direct and multipath arrivals are separated and (2) the arrivals from successive calls do not overlap. Where the calls overlap, the location method requires user supervision to identify locations where all the arrival times appear to be from one call. The double-difference relative relocation technique (Waldhauser and Ellsworth, 2000) is widely used in earthquake studies and seems well suited to relocating closely spaced marine mammal calls with consistent waveforms. For fin whales the relative location errors obtained within our network with this method are comparable to the length of the whale.

ACKNOWLEDGMENTS

The author thanks two anonymous reviewers for insightful comments that substantially improved the manuscript and John Delaney, Emilie Hooft, Deborah Kelley, Paul McGill, Debra Stakes, and Douglas Toomey for their contributions to the data collection. The seismic data collection was funded by the W. M. Keck Foundation and this research by the Office of Naval Research under Grant No. N00014-08-1-0523.

- Aki, K. (1967). "Scaling law of seismic spectrum," *J. Geophys. Res.* **72**, 1217–1231.
- Baggenstoss, P. M. (2011). "An algorithm for the localization of multiple interfering sperm whales using multi-sensor time difference of arrival," *J. Acoust. Soc. Am.* **130**, 102–112.
- Bowlin, J. B., Spiesberger, J. L., Duda, T. F., and Freitag, L. F. (1993). "Ocean acoustical ray-tracing software RAY," Woods Hole Oceanographic Institution Technical Report No. WHOI-93-10, Woods Hole, MA.
- Bracewell, R. N. (1978). *The Fourier Transform and its Applications* (McGraw-Hill, New York), pp. 267–271.
- Christeson, G. L., Purdy, G. M., and Fryer, G. J. (1994). "Seismic constraints on shallow crustal emplacement processes at the fast spreading East Pacific Rise," *J. Geophys. Res.* **99**, 17957–17973.
- Clark, C. W., Borsani, J. F., and Notarbartolo di Sciarra, G. (2002). "Vocal activity of fin whales, *Balaenoptera physalus*, in the Ligurian Sea," *Marine Mammal Sci.* **18**, 286–295.
- Dunn, R. A., and Hernandez, O. (2009). "Tracking blue whales in the eastern tropical Pacific with an ocean-bottom seismometer and hydrophone array," *J. Acoust. Soc. Am.* **126**, 1084–1094.
- Fox, C. G., Matsumoto, H., and Lau, T. A. (2001). "Monitoring Pacific Ocean seismicity from an autonomous hydrophone array," *J. Geophys. Res.* **106**, 4183–4206.
- Frank, S. D., and Ferris, A. N. (2011). "Analysis and localization of blue whale vocalizations in the Solomon Sea using waveform amplitude data," *J. Acoust. Soc. Am.* **130**, 731–736.
- Gilbert, L. A., and Johnson, H. P. (1999). "Direct measurements of oceanic crustal density at the Northern Juan de Fuca Ridge," *Geophys. Res. Lett.* **26**, 3633–3636.
- Greene, C. R., Jr., McLennan, M. W., Norman, R. G., McDonald, T. L., and Richardson, W. J. (2004). "Directional frequency and recording (DIFAR) sensors in seafloor recorders to locate calling bowhead whales during their fall migration," *J. Acoust. Soc. Am.* **116**, 799–813.
- Ikelle, L. T., and Amundsen, L. (2005). *Introduction to Petroleum Seismology* (Society for Exploration Geophysics, Tulsa, OK), pp. 92–95.
- Ioup, G. E., Ioup, J. W., Tashmukhambetov, A. M., Pflug, L. A., Newcomb, J. J., Sidorovskaia, N. A., Kuczaj, S. A., Rayborn, G. H., Stephens, J. M., Tiemann, C. O., and Bernstein, A. (2009). "Environmental acoustic recording system (EARS) buoys for marine animal acoustics," *J. Acoust. Soc. Am.* **125**, 2616.
- Karsten, J. L., Hammond, S. R., Davis, E. E., and Currie, R. G. (1986). "Detailed geomorphology and neotectonics of the Endeavour segment, Juan de Fuca Ridge: New results from Seabeam swath mapping," *Geol. Soc. Am. Bull.* **97**, 213–221.
- Lammers, M. O., Brainard, R. E., Whitlow, W. L. A., Aran Mooney, T., and Wong, K. B. (2008). "An ecological acoustic recorder (EAR) for long-term monitoring of biological and anthropogenic sounds on coral reefs and other marine habitats," *J. Acoust. Soc. Am.* **123**, 1720–1728.
- Lee, W. H. K., and Stewart, S. W. (1981). *Principles and Applications of Microearthquake Networks* (Academic Press, New York).
- Levitus, S. (1982). *Climatological Atlas of the World Ocean* (U.S. Government Printing Office, Washington, DC).
- McDonald, M. A., Hildebrand, J. A., and Webb, S. C. (1995). "Blue and fin whales observed on a seafloor array in the Northeast Pacific," *J. Acoust. Soc. Am.* **98**, 712–721.
- McManus, D. A., Holmes, M. L., Carson, B., and Barr, S. M. (1972). "Late Quaternary tectonics, northern end of Juan de Fuca Ridge (northeast Pacific)," *Marine Geol.* **12**, 141–164.
- Mellinger, D. K., and Clark, C. W. (1997). "Methods for automatic detection of mysticete sounds," *Marine Freshwater Beh. Physiol.* **29**, 163–181.
- Moore, S. E., Stafford, K. M., Mellinger, D. K., and Hildebrand, J. A. (2006). "Listening to large whales in the offshore waters of Alaska," *BioSci.* **56**, 49–55.
- Morrissey, R. P., Ward, J., DiMarzio, N., Jarvis, S., and Moretti, D. J. (2006). "Passive acoustic detection and localization of sperm whales (*Physeter macrocephalus*) in the tongue of the ocean," *Appl. Acoust.* **67**, 1091–1105.
- Muoy, X., Bahoura, M., and Simard, Y. (2009). "Automatic recognition of fin and blue whales calls for real-time monitoring in the St Lawrence," *J. Acoust. Soc. Am.* **126**, 2918–2928.
- Nosal, E.-M., and Frazer, L. N. (2006). "Track of a sperm whale from delays between direct and surface-reflected clicks," *Appl. Acoust.* **67**, 1187–1201.
- Nosal, E.-M., and Frazer, L. N. (2007). "Modified pariwise spectrogram processing for localization of unknown broadband sensors," *IEEE J. Ocean Eng.* **32**, 721–728.
- Paige, C. C., and Saunders, M. A. (1982). "LSQR: An algorithm for sparse linear equations and sparse least squares," *ACM Trans. Math. Software* **8**, 43–71.
- Rebull, O. G., Cusi, J. D., Fernandez, M. R., and Muset, J. G. (2006). "Tracking fin whale calls offshore the Galicia Margin, NE Atlantic Ocean," *J. Acoust. Soc. Am.* **120**, 2077–2085.
- Romanowicz, B., Stakes, D., Uhrhammer, R., McGill, P., Neuhauser, D., Ramirez, T., and Dolenc, D. (2003). "The MOBB experiment: A prototype permanent off-shore ocean bottom broadband station," *Eos Trans. AGU* **84**, 325, 331–332.
- Schaff, D. P., Bokelmann, G. H. R., Ellsworth, W. L., Zankerka, E., Waldhauser, F., and Beroza, G. C. (2004). "Optimizing correlation techniques for improved earthquake location," *Bull. Seismol. Soc. Am.* **94**, 705–721.
- Schevill, W. E., Watkins, W. A., and Backus, R. H. (1964). "The 20-cycle signals and *Balaenoptera* (fin whales)," in *Marine Bio-Acoustics*, edited by W. N. Tavalgo (Pergamon, Oxford), pp. 147–152.
- Soule, D. C., Wilcock, W. S. D., and Thomson, R. E. (2009). "Distribution of fin and blue whales above hydrothermal vent fields on the Juan de Fuca Ridge, northeast Pacific Ocean," in 18th Biennial Conference on the Biology of Marine Mammals (Quebec City, Canada).
- Speisberger, J. L., and Fristrup, K. M. (1990). "Passive location of calling animals and sensing of their acoustic environment using acoustic tomography," *Am. Nat.* **135**, 107–153.
- Stakes, D., McClain, J., Van Zandt, T., McGill, P., and Begnaud, M. (1998). "Corehole seismometer development for low-noise seismic data in a long-term seafloor observatory," *Geophys. Res. Lett.* **25**, 2745–2748.
- Sun, Y. F. (2000). "Core-log-seismic integration in hemipelagic marine sediments on the eastern flank of the Juan de Fuca Ridge," *Proc. ODP Sci. Results* **168**, 21–35.
- Thompson, P. O., Findlay, L. T., and Vidal, O. (1992). "20-Hz pulses and other vocalizations of fin whales, *Balaenoptera physalus*, in the Gulf of California, Mexico," *J. Acoust. Soc. Am.* **92**, 3051–3057.
- Tiemann, C. O., Porter, M. B., and Frazer, L. N. (2004). "Localization of marine mammals near Hawaii using an acoustic propagation model," *J. Acoust. Soc. Am.* **115**, 2834–2843.
- VanDecar, J. C., and Crosson, R. S. (1990). "Determination of teleseismic relative phase arrival times using multi-channel cross-correlation and least squares," *Bull. Seismol. Soc. Am.* **80**, 150–169.
- Waldhauser, F. (2001). "hypoDD—A program to compute double-difference hypocenter locations," United States Geological Survey Open File Rep. 01–113, Menlo park, CA.
- Waldhauser, F., and Ellsworth, W. L. (2000). "A double-difference earthquake location algorithm: Method and application to the northern Hayward Fault, California," *Bull. Seismol. Soc. Am.* **90**, 1353–1368.
- Walker, R. A. (1963). "Some intense, low-frequency, underwater sounds of wide geographic distribution, apparently of biological origin," *J. Acoust. Soc. Am.* **35**, 1816–1824.
- Watkins, W. A., Tyack, P., and Moore, K. E. (1987). "The 20-Hz signals of finback whales (*Balaenoptera physalus*)," *J. Acoust. Soc. Am.* **82**, 1901–1912.
- Wiggins, S. M. (2003). "Autonomous acoustic recording packages (ARPs) for long-term monitoring of whale sounds," *Marine Technol. Soc. J.* **37**, 13–22.
- Wilcock, W. S. D., Hooft, E. E. E., Toomey, D. R., McGill, P. R., Barclay, A. H., Stakes, D. S., and Ramirez, T. M. (2009). "The role of magma injection in localizing black smoker activity," *Nat. Geosci.* **2**, 509–513.
- Wilcock, W. S. D., McGill, P. R., Hooft, E. E. E., Toomey, D. R., Patel, H. M., Stakes, D. S., Barclay, A. H., Ramirez, T. M., and Weekly, R. T. (2007). "The deployment of a long-term seismic network on the Juan de Fuca Ridge," in *MTS/IEEE Oceans 2007 Meeting*, Vancouver, Canada.
- Wilcock, W. S. D., and Toomey, D. R. (1991). "Estimating hypocentral uncertainties from marine microearthquake surveys: A comparison of generalized inverse and grid search methods," *Marine Geophys. Res.* **13**, 161–171.
- Zimmer, W. X. Z. (2011). *Passive Acoustic Monitoring of Cetaceans* (Cambridge University Press, New York).